Hydraulics of Rectangular Dropshafts

H. Chanson[1]

Abstract: A dropshaft is an energy dissipator connecting two channels with a drop in invert elevation. The hydraulics of vertical rectangular shafts was systematically investigated in seven configurations. A particular emphasis was on the effects of shaft pool, outflow direction, and drop height, while geometrically similar shafts (scale 3.1:1) were studied using a Froude similitude. The results demonstrate that rectangular dropshafts with 90° outflow are the most efficient energy dissipators. The shaft pool and drop height have little effect on the rate of energy dissipation. Recirculation time results exhibited marked differences between flow regimes and the longest dimensionless residence times were observed at low flow rates. Although basic flow characteristics were similar between model and prototype, observations of dimensionless bubble penetration depths and recirculation times showed some discrepancy, highlighting limitations of the Froude similitude for studies of air entrainment and residence times in dropshafts.

DOI: 10.1061/(ASCE)0733-9437(2004)130:6(523)

CE Database subject headings: Energy dissipation; Hydraulics; Recirculation; Channel flow; Flow rates.

Introduction

A dropshaft is an energy dissipator connecting two channels with a drop in invert elevation (Figs. 1 and 2). It is an ancient design: e.g., the dropshaft cascades along Roman aqueducts (e.g., Roidot-Deléage 1879; Leveau and Paillet 1976; Lopez-Cuervo 1985; Chanson 2002a). Dropshafts are commonly used in sewers, storm-water systems, and downstream of culverts, and large spillway shafts were built (Apelt 1984; Rajaratnam et al. 1997). Fig. 1 shows a dropshaft downstream of a road culvert. Despite such long usage, the hydraulics of dropshafts has not been systematically documented (Merlein et al. 2002).

It is the purpose of this paper to detail the hydraulic characteristics of rectangular dropshafts. New measurements were performed systematically with several geometries, with a particular emphasis on the effects of shaft pool, outflow direction, and drop height. The data are compared with existing data sets. The results provide an unique characterization of the hydraulic performances of rectangular dropshafts as well some insights into scale effects associated with physical modeling.

Experimental Apparatus

Seven dropshafts were studied in two flumes (Table 1). The vertical shafts were built in marine plywood and perspex (Fig. 3). The upstream horizontal channels were open while the downstream horizontal conduits were covered and ended with a free overfall.

The five smallest shafts were designed to investigate systematically the effects of shaft pool (P=0 and 0.32 m), outflow direction (ϕ=90 and 180°), and drop height (h=0.55 and 0.87 m), where P is the pool height, ϕ is the outflow direction angle, and h is the drop in invert elevation (Table 1). For two geometries, two geometrically scaled shafts were built and tested. These were the prototype P1 corresponding to model M4 and the prototype P2 corresponding to model M5 (Table 1). They were designed to be geometrically similar based upon a Froude similitude with undistorted scale (e.g., Henderson 1966; Chanson 1999). In each case, the geometric scaling ratio was L_R=3.1. Similar experiments were conducted for identical dimensionless inflow critical depth d_c/h, where d_c is the critical depth at the brink and h is the invert drop in elevation (Fig. 2). Measurements were performed at similar locations.

Instrumentation

In the smallest shaft experiments, the discharges were deduced from brink depth measurements that were first calibrated in situ with volume-per-time discharge data. In the largest dropshafts, flows rates were estimated from bend meters which were calibrated in situ with a 90° V-notch weir.

Free-surface elevations were recorded with pointer gauges while the free-surface height in the shaft was measured with rulers. The total head was measured with a total head tube (∅ =1 mm). Measurements were conducted at five transverse profiles and averaged over the cross section. The averaging method was particularly important with the 90° outflow direction configurations.

Additional information was obtained with high-speed photography and video camera (e.g., Figs. 3 and 7). Further details on the experimental facilities and data were reported in Chanson (2002b).

Recirculation Times

Recirculation times in the shaft were recorded using neutrally buoyant particles (relative density 0.95 to 1.05) made of wax and

[1]Reader, Environmental Fluid Mechanics and Hydraulic Engineering, Dept. of Civil Engineering, Univ. of Queensland, Brisbane QLD 4072, Australia.

Note. Discussion open until May 1, 2005. Separate discussions must be submitted for individual papers. To extend the closing date by one month, a written request must be filed with the ASCE Managing Editor. The manuscript for this paper was submitted for review and possible publication on February 27, 2003; approved on June 10, 2003. This paper is part of the ***Journal of Irrigation and Drainage Engineering***, Vol. 130, No. 6, December 1, 2004. ©ASCE, ISSN 0733-9437/2004/6-523–529/ $18.00.

aluminium to study the recirculation process in the shaft configurations with pool ($P>0$). In the smallest shafts, particles with sizes of 3.3, 3.9, 5, and 9 mm were used, while observations in the largest shaft were made with particle sizes of 5, 9 and 15 mm. The particle travel times were recorded with digital chronometers. Residence times in the shafts were deduced by subtracting the calculated travel times in the inflow and outflow channels to the total measured time. Experiments were repeated with three to four particle sizes for each shaft configuration and flow rate, and for at least 40 to 50 times with each particle size.

Basic Flow Patterns

For shafts with 180° outflow direction, three basic flow patterns were observed as functions of the flow rate and shaft configurations (Fig. 2). These were consistent with the earlier observations of Rajaratnam et al. (1997) and Chanson (2002a). At low flow rates, the free-falling nappe impacted into the shaft pool at low flow rates (Regime R1). Large numbers of air bubbles were entrained at nappe impingement and seen recirculating in the shaft pool. For intermediate discharges, the nappe impacted into the downstream channel invert (Regime R2). Very strong pressure fluctuations were felt on the outflow channel invert, and splashing and spray was significant downstream of nappe impact (Fig. 2). At large flow rates, the nappe impacted onto the opposite wall above the downstream conduit obvert (Regime R3). [The *obvert*, or soffit, is the roof of a closed conduit; the term is commonly used in culvert design (e.g., Chanson 1999).] Nappe impact was associated with formation of a roller described by Renner (1973, 1975). Beneath the nappe impact, water ran downward along the wall and the central section was deflected into the downstream conduit as a high-velocity shooting flow. These observations were consistently noted in both models and prototypes.

For a 90° shaft configuration, the above observations were generally valid, but Regime R2 did not exist. Only Regimes R1 and R3 were observed.

With deep shaft pools ($P>0$), strong flow recirculation was clearly observed in the shaft pool for all flow regimes. In the shafts with no pool ($P=0$) the above observations were basically valid, but air entrainment and flow recirculation in the shaft pool were limited by the shaft invert. However, greater splashing was visually noticed in the shaft [Fig. 3(b)].

The transitions between flow regimes were recorded. Results are presented in Tables 2 and 3 and compared with previous observations. Note that the experimental observations compared favorably with nappe trajectory calculations.

Fig. 1. Dropshaft downstream of a road culvert in Coolum, Queensland, on November 18, 2002. The shaft is a vertical concrete pipe. A manhole is seen at the top of the shaft (top right of photograph), and the outflow pipe ($\varnothing \sim 1$ m) is in the foreground bottom left.

Table 1. Experimental Investigations of Rectangular Dropshafts

Reference	h m	P m	L m	B m	l m	b_1 m	D_1[a] m	b^2 m	D_2 m	Outflow direction ϕ (°)	Remark
Present study	2.70	0	0.755	0.763	0.12	0.50	0.30	0.65	0.20	90	Prototype P1
	1.70	1.00	0.755	0.763	0.12	0.50	0.30	0.50	0.30	180	Prototype P2
	0.87	0	0.243	0.246	0.039	0.161	0.25	0.209	0.064	90	Model M4
	0.548	0.322	0.243	0.246	0.039	0.161	0.25	0.209	0.097	180	Model M5
	0.548	0.322	0.243	0.246	0.039	0.161	0.25	0.209	0.097	90	Model M6
	0.548	0	0.243	0.246	0.039	0.161	0.25	0.209	0.097	180	Model M7
	0.548	0	0.243	0.246	0.039	0.161	0.25	0.209	0.097	90	Model M8
Chanson (2002a)	0.505	0.365	0.30	0.30	0	0.144	0.25	0.15	0.25	180	Recret model
	0.668	0.201	0.20	0.30	0	0.110	0.25	0.11	0.21	90	Valdepuentes 1
	0.668	0.201	0.20	0.30	0	0.110	0.25	0.11	0.21	180	Valdepuentes 2
Apelt (1984)	0.325	0	0.152	0.152	0	Pipe: $\varnothing$=0.152 m		Pipe: $\varnothing$=0.152 m		180	

[a]Sidewall height; Notation: see Fig. 2.

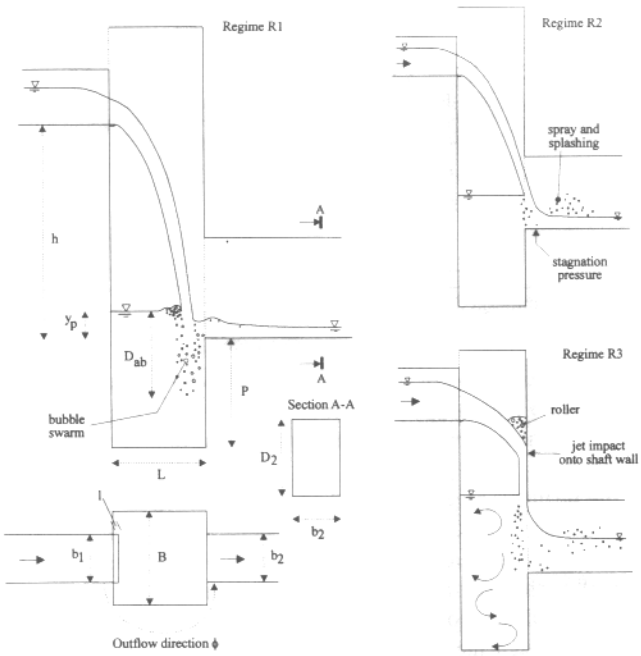

Fig. 2. Basic flow patterns for a rectangular dropshaft with 180° outflow direction

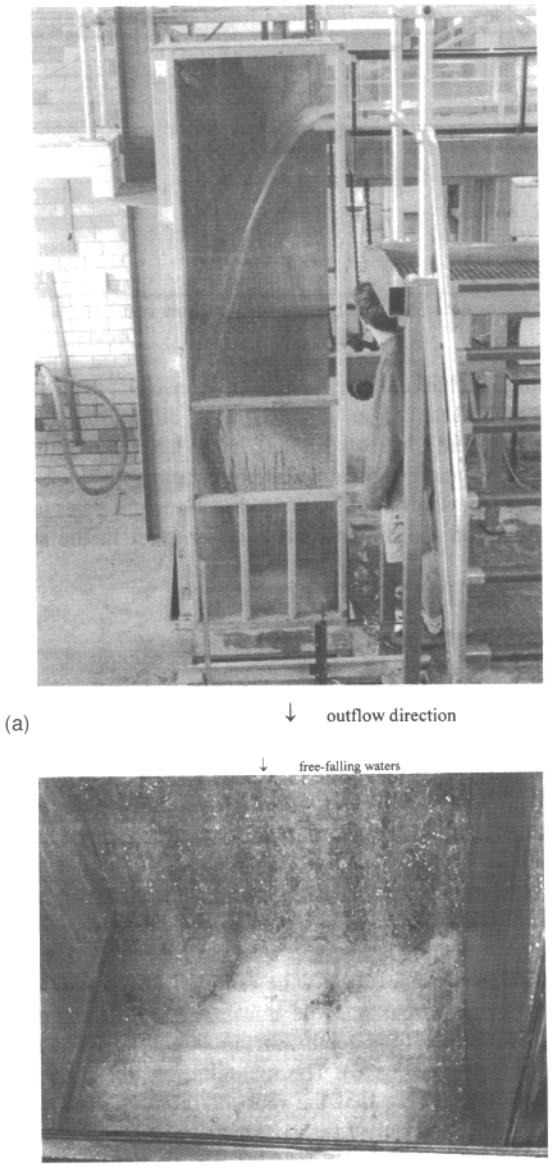

Fig. 3. Rectangular dropshaft configuration P1 (h=2.7 m, ϕ=90°) in Regime R3: (a) Side view; (b) looking downward into the shaft (at bottom end, the flow turns 90° to the right)

Remarks

For all investigated flow conditions, the upstream channel operated as free-surface flow corresponding to subcritical inflow conditions, while the downstream channel operated always with supercritical flows. Rajaratnam et al. (1997) and Chanson (2002a) reported a similar finding.

Hydraulic Properties

Residual Energy

Residual energy data are presented in Fig. 4. The data are shown in terms of the dimensionless residual head H_2/H_1 as a function of the dimensionless flow rate d_c/h, where H_2 is the specific energy in the downstream channel and H_1 is the upstream total head measured above the downstream channel invert. Fig. 4(a) presents results obtained for shafts with deep pools and 180° outflow direction, and these are compared with an earlier study. Excellent rates of energy dissipation were observed at low flow rates (i.e., Regime R1). Poor dissipation performances occurred in Regime R2. At large flow rates (Regime R3), the dimensionless residual head results were intermediate between regimes R1 and R2 performances. Note the relatively good agreement between model and prototype data.

Effects of Pool Depth and Outflow Direction

The effects of pool depth, outflow direction, and shaft height were systematically investigated, all other dropshaft parameters being kept constant. Results are presented in Figs. 4(b and c). The comparison shows that the absence (or presence) of pool had little effect on the residual energy, but a greater rate of energy dissipation was observed with the 90° outflow direction, all other parameters being identical. The result is illustrated in Fig. 4(b), where the dimensionless residual heads in Models 6 and 8 (ϕ=90°, white symbols) are consistently smaller than those measured in Models 5 and 7 (ϕ=180°, cross symbols), particularly for $d_c/h > 0.04$. The findings agree with Chanson's (2002a) data on the Valdepuentes dropshaft models.

Fig. 4(c) compares energy dissipation performances of three dropshafts without pool and with 90° outflow direction. The results suggest little effect of the shaft height on the dimensionless residual head for these configurations (P=0, ϕ=90°).

Pool Free-Surface Height

Dimensionless pool free-surface height data are reported in Fig. 5 as y_p/D_2 as a function of the dimensionless discharge d_c/h, where y_p is the free-surface height above downstream invert and D_2 is the downstream conduit height (Fig. 2). For $y_p/D_2 > 1$, the outflow channel invert is submerged. Model and prototype data exhibit a close trend, highlighting an increase in pool height with

Table 2. Flow Conditions d_c/h for Change in Flow Regimes (180° Shaft Configurations)

	d_c/h transition			
Configuration	R1-R2	R2-R3a	R3a-R3b	Remarks
Prototype P2	0.037	0.046	—	P=1.0 m
Model M5	0.039	0.051	0.10	P=0.32 m
Model M7	0.038	0.046	0.099	P=0
Recret model	0.09	0.175	—	P=0.36 m Chanson (2002a)
Valdepuentes 2	0.029	0.042	—	P=0.20 m Chanson (2002a)

Note: R3a=regime R3 with free-surface outflow channel inlet; and R3b=regime R3 with submerged outflow channel inlet.

increasing discharges. The results are consistent with the observations of Rajaratnam et al. (1997), but differ from the data of Apelt (1984) and Chanson (2002a). In the latter, the outflow channel was taller and the obvert was not submerged.

Overall, the shaft pool, outflow direction, and shaft height had little effects on the dimensionless water level in the shaft pool (Fig. 5).

Bubble Penetration Depth

Bubble-swarm depths D_{ab} were visually recorded for dropshaft configurations with deep shaft pool ($P>0$, Table 1). Dimensionless penetration depth $D_{ab}/(y_p+P)$ are presented in Fig. 6 as a function of the dimensionless flow rate d_c/h, where (y_p+P) is the water depth in the shaft. Substantial flow aeration was observed in Regimes R1 and R3, and the bubble cloud occupied a sizeable pool volume. The flow regime R2 was less efficient in entraining air because the nappe did not impact in the pool but interacted with the downstream conduit inlet. In configurations with 90 outflow direction, the Regime R2 was not experienced and strong flow aeration was seen for a wide range of flow conditions.

Visual observations showed consistently smaller dimensionless bubble penetration depths in the prototype P2 than in the similar model M5 (Fig. 6). The magnitude of the discrepancy is staggering considering that the ratio of prototype (P2) to model (M5) dimensions is only L_R=3.1. This visual, subjective result is likely to be related to some form of scale effects, as indeed air entrainment cannot be scaled with a Froude similitude (Wood 1991; Chanson 1997).

Recirculation Times

Visual observations highlighted strong vortical motion and flow recirculation in the shaft pool for all dropshaft configurations with deep pool ($P>0$). Fig. 7 illustrates strong turbulence in a shaft pool for flow regime R1. It is believed that turbulent motion in the pool contributes to a significant amount of energy dissipation. In turn, a quantification of the recirculation times may provide some insights into the dissipative processes. (The recirculation time is defined as the residence time of neutrally buoyant particles in the shaft.)

The results showed that the data were basically independent of the particle sizes (3.3 to 9 mm in models, 5 to 15 mm in prototypes) for all flow regimes and configurations (Chanson 2002b). Thereafter the data are regrouped for all particle sizes. The experimental data showed marked differences between flow regimes, although the probability distribution functions of dimensionless residence time were basically independent of the flow rate for one dropshaft configuration and one flow regime. At low flow rates (Regime R1), the dimensionless particle residence time was comparatively the greatest, corresponding to the entrainment of particles in the shaft pool and their trapping in large-size vortical structures for a significant duration [Figs. 8(a and c)]. At intermediate discharges (Regime R2), the free-falling nappe flowed directly into the outflow channel. Most particles were directly entrained into the outflow conduit with a very small residence time. At large flow rates (Regime R3), particles were sometimes entrained down the shaft pool, but most exited the shaft rapidly [Figs. 8(b and d)]. The same trends were observed in models and prototype. Typical results are presented in Fig. 8. Each graph shows the normalized probability distribution function of dimensionless residence times T^*d_c/V_c, where T is the recirculation time and V_c is the critical velocity. Note that Figs. 8(a and c) have the same horizontal scale, while Figs. 8(b and d) have a different horizontal axis scale. This reflects marked differences between Regimes R1 and R3 results.

Figs. 8(a and b) compare dimensionless recirculation times for two identical model dropshafts, other than the outflow direction (ϕ=90° and 180°). The average particle residence times were smaller with a 90° outflow direction than those in the 180° outflow direction configuration, all other parameters being identical. In dropshafts with 90° outflow direction, particles had to be subjected to change in flow direction before exiting the shaft. Visually most particles tended to be entrained deep down the pool shaft, to turn around near the shaft bottom and to flow outwards

Table 3. Flow Conditions d_c/h for Change in Flow Regimes (90° Shaft Configurations)

	d_c/h transition		
Configuration	R1-R3a	R3a-R3b	Remarks
Prototype P1	0.013	—	P=0
Model M4	0.017	0.060	P=0
Model M6	0.037	0.12	P=0.32 m
Model M8	0.035	0.11	P=0
Valdepuentes 1	0.028	—	P=0.2 m Chanson (2002a)

Note: R3a=regime R3 with free-surface outflow channel inlet; and R3b=regime R3 with submerged outflow channel inlet.

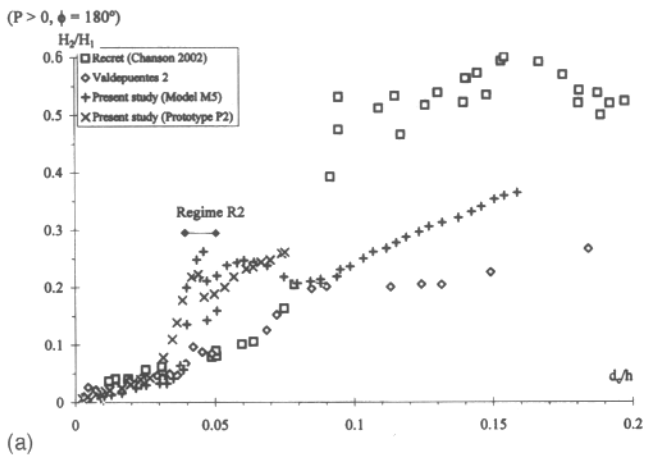

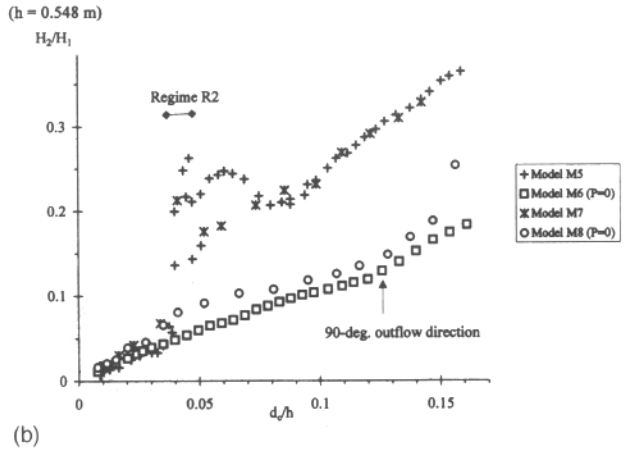

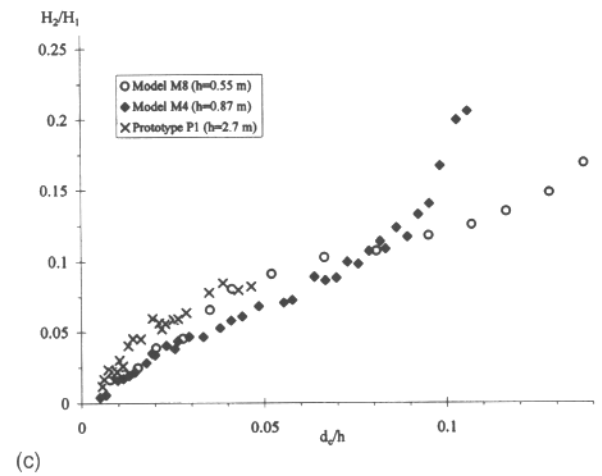

Fig. 4. Dimensionless residual head H_2/H_1 as a function of the dimensionless flow rate d_c/h: (a) Scale effects—comparison between prototype P2, models M5, and Chanson's (2002a) models ($P>0$, $\phi=180°$); (b) effects of shaft pool and outflow direction—comparison between models M5, M6, M7, and M8 ($h=0.548$ m); (c) effects of drop in invert elevation—comparison between models M4 and M8 ($P=0$, $\phi=90°$)

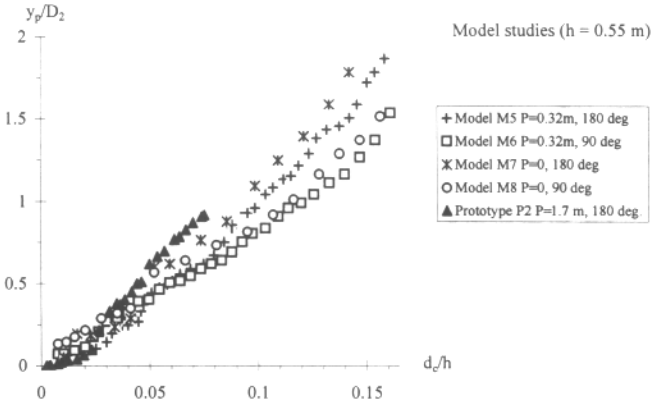

Fig. 5. Dimensionless pool height y_p/D as a function of the dimensionless flow rate d_c/h

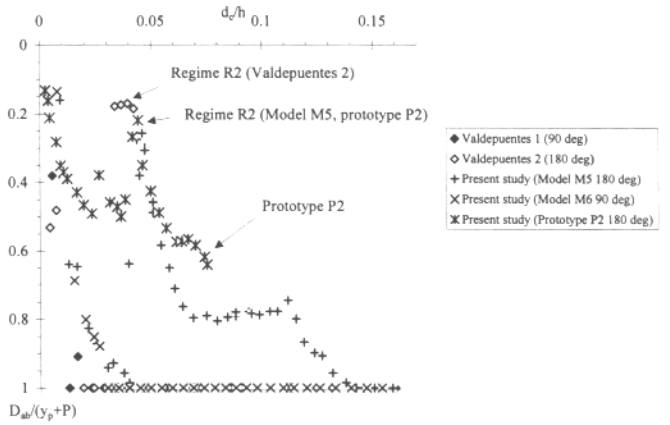

Fig. 6. Dimensionless bubble penetration depth $D_{ab}/(y_p+P)$ as a function of the dimensionless flow rate d_c/h; effects of outflow direction and scales—comparison between models M5 and M6, prototype P2 and the data of Chanson (2002a) for deep shaft pools ($P>0$)

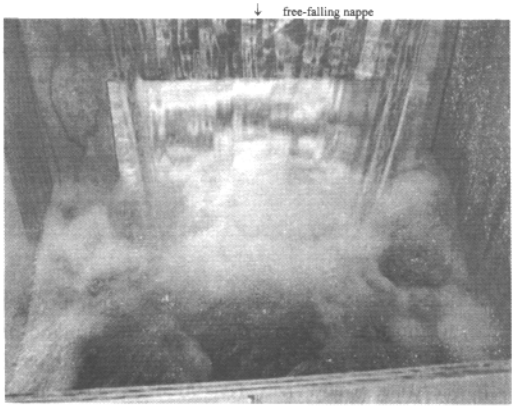

Fig. 7. Flow recirculation in the shaft pool—Prototype P2, Regime R1—looking from under the inflow channel toward the pool free-surface with the outflow channel in background; note the free-falling nappe and the bubbly foam at the free-surface of the pool

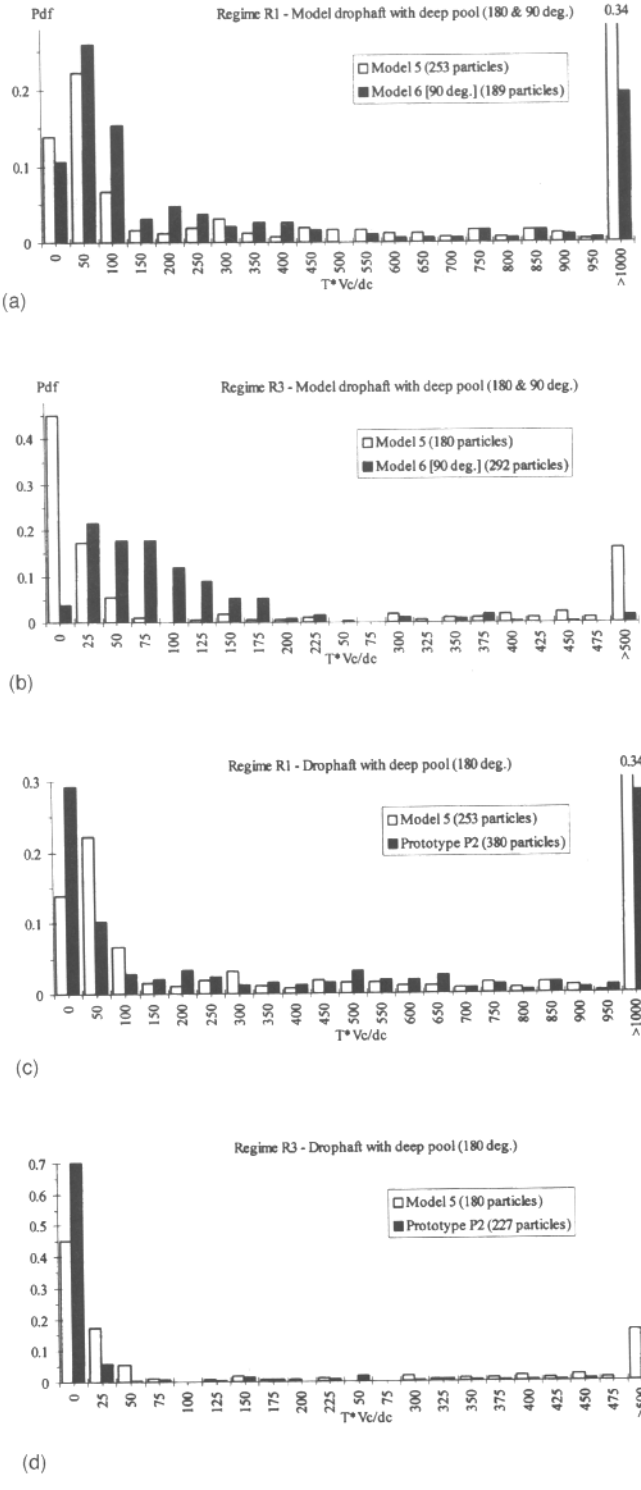

Fig. 8. Probability distribution functions of dimensionless residence time $T^* V_c/d_c$—comparison between models M5, M6, and prototype P2 ($P>0$): (a) Effect of outflow direction—comparison between models M5 ($\phi=180°$) and M6 ($\phi=90°$) in flow regime R1; (b) effect of outflow direction—comparison between models M5 ($\phi=180°$) and M6 ($\phi=90°$) in flow regime R3; (c) scale effects—comparison between model M5 and Prototype P2 ($\phi=180°$) in flow regime R1; (d) scale effects—comparison between model M5 and Prototype P2 ($\phi=180°$) in flow regime R3

rapidly. The same pattern was observed in Regimes R1 and R3.

Figs. 8(c and d) compare the performances of two geometrically similar configurations with 180° outflow direction, i.e., model M5 and prototype P2. With small discharges (Regime R1), the residence time probability distributions exhibited a bimodal shape. About 40–50% of the particles flowed downward at nappe impact and were rapidly entrained downstream (Mode 1). The rest of the particles were trapped in large-scale vortices (Mode 2). They were seen to recirculate in large-scale flow structures, sometimes passing from one structure to another, until they were finally entrained in the downstream conduit. For the data shown in Fig. 8(a), the Model 1 data were centered around $T^* V_c/d_c=66$ and 33 for model and prototype, respectively, while Model 2 data were centred roughly around $T^* V_c/d_c=1770$ and 1230 for model M5 and prototype P2. In Figs. 8(c and d), the data suggest similar trends in model and prototype, although prototype results suggest smaller dimensionless residence times for all flow regimes. Such observations suggest some form of scale effects. It is believed that recirculation times are strongly related to vortical motion in the shaft pool, which cannot be scaled by a Froude similitude.

Summary and Conclusions

The hydraulics of vertical rectangular dropshafts was systematically investigated in seven configurations. A particular emphasis was on the effects of shaft pool, outflow direction, and drop height, while geometrically similar shafts (scale 3.1:1) were studied using an undistorted Froude similitude for two geometries.

Experimental observations showed distinct flow regimes associated with nappe impact in the shaft pool, in the outflow channel, or in the opposite shaft wall (Fig. 2). The rate of energy dissipation was nearly 95% at low flow rates (Regime R1). The pool depth and shaft height had little effect on the rate of energy dissipation, but larger energy dissipation rates were consistently observed with 90° outflow direction configurations. Practically, the results demonstrate that rectangular dropshafts with 90° outflow are more efficient energy dissipators. The shaft pool and drop height have little effect on the rate of energy dissipation. Neutrally buoyant particles were used to estimate recirculation times. The results exhibited marked differences between flow regimes, and the longest dimensionless residence times were observed at low flow rates (Regime R1).

Although basic hydraulic characteristics were similar between model and prototype based upon a Froude similitude (scale ratio $L_R=3.1$), observations of dimensionless bubble penetration depths and recirculation times presented marked differences between model and prototype results. It is believed that these highlight some limitations of the Froude similitude for studies of air entrainment, residence times, and mass transfer in dropshaft.

While present experiments were conducted with almost square shafts, the results are likely to apply to circular dropshafts with rectangular inflow and outflow channels with ratio of outflow channel width to shaft diameter of about 0.6 to 0.7.

Acknowledgments

The writer thanks his students J. I. Wilson and C. Russell. He acknowledges the technical assistance of Graham Illidge.

Notation

The following symbols are used in this paper:

B = shaft breadth (m);
b = channel breadth (m);
D = channel height (m);
D_{ab} = bubble penetration depth (m);
d = water depth (m);
d_c = critical depth (m);
H = total head (m);
h = drop height (m);
L = shaft length (m);
L_R = geometric scaling ratio, i.e., ratio of prototype to model dimensions;
P = shaft pool height (m)
Q = water discharge (m^3/s) in culvert;
T = recirculation time (s);
V_c = critical flow velocity (m/s);
S_o = bed slope;
y_p = pool height above downstream channel invert (m);
ϕ = outflow direction angle; and
$\varnothing$ = diameter (m).

References

Apelt, C. J. (1984). "Goonyella railway duplication drop structures and energy dissipators at culvert outlets. Model studies." *Rep. CH27/84*, Dept. of Civil Engineering, Univ. of Queensland, Australia, Feb.

Chanson, H. (1997). "*Air bubble entrainment in free-surface turbulent shear flows*," Academic, London.

Chanson, H. (1999). "*The hydraulics of open channel flows: An introduction*," Butterworth-Heinemann, Oxford, U.K.

Chanson, H. (2002a). "An experimental study of Roman dropshaft hydraulics." *J. Hydraul. Res.*, 40(1), 3–12.

Chanson, H. (2002b). "An experimental study of Roman dropshaft operation: Hydraulics, two-phase flow, acoustics." *Rep. CH50/02*, Dept of Civil Engineering, Univ. of Queensland, Brisbane, Australia.

Henderson, F. M. (1966). "*Open channel flow*," MacMillan, New York.

Leveau, P., and Paillet, J. L. (1976). "L'Alimentation en Eau de Caesarea de Maurétanie et l'Aqueduc de Cherchell." ("The water supply of Caesarea of Mauretanie and the Cherchell aqueduct.") Librairie Edition L'Harmattan, Paris (in French).

Lopez-Cuervo, S. (1985). "Medina Az-Zahra Ingeniera y Formas." *Publicaciones del Ministerio de Obras Publicas y Urbanismo*, Madrid, Spain (in Spanish).

Merlein, J., Kleinschroth, A., and Valentin, F. (2002). "Systematisierung von Absturzbauwerken." *Mitterilung No. 69*, Lehrstuhls fur Hydraulik und Gewasserkunde, Technishen Universitat Munchen, Germany.

Rajaratnam, N., Mainali, A., and Hsung, C. Y. (1997). "Observations on flow in vertical dropshafts in urban drainage systems." *J. Environ. Eng.*, ASCE, 123(5), 486–491.

Renner, J. (1973). "Lufteinmischung beim Aufprall eines ebenen Wasserstrahls auf eine Wand." ("Air entrainment by a plane water jet impinging on a wall.") PhD thesis, Univ. of Karsruhe, Germany (in German).

Renner, J. (1975). "Air entrainment in surface rollers." *Proc., Symposium on Design and Operation of Siphons and Siphon Spillways*, BHRA Fluid Engineers, London.

Roidot-Deléage, J. (1879). "Autun ancient et moderne," (Autun ancient and modern) Société Éduenne, Autun, France (in French).

Wood, I. R. (1991). "*Air entertainment in free-surface flows*," IAHR hydraulic structures design manual No. 4, Hydraulic design considerations, Balkema, Rotterdam, The Netherlands.